Energy Reports 8 (2022) 2302–2313

Contents lists available at ScienceDirect

Energy Reports

journal homepage: www.elsevier.com/locate/egyr

Research paper

Effects of induction machine parameters on its performance as a standalone self excited induction generator

M. Faisal Khan [a,b], M. Rizwan Khan [c,b], Atif Iqbal [d,*]

[a] EES, University Polytechnic, F/O Engg. & Tech.
[b] Aligarh Muslim University, Aligarh 202002, India
[c] EED, Z. H. College oF Engg. and Tech., F/O Engg. & Tech.
[d] Department of Electrical Engineering, Qatar University, Qatar

ARTICLE INFO

Article history:
Received 17 October 2021
Received in revised form 5 January 2022
Accepted 7 January 2022
Available online xxxx

Keywords:
Self excited induction generator
Moment of inertia
Stator resistance
Parametric influence
Saturation modeling

ABSTRACT

A squirrel cage induction machine (SCIM) when aggregated with relevant capacitances and a prime mover, acts as self-excited induction generator (SEIG). As it hosts energy conversion the parameters of SCIM have considerable impact on the power extraction capability of SEIG. An aspect which is missing from the available research on SEIGs is evaluation of the affects of its rotor's moment of inertia (J) and per-phase stator winding resistance (R_s) on performance indices. This work investigates the impacts of these factors on a SCIM's performance as series compensated, short shunt SEIG. The study considers two distinctly designed SCIMs, in terms of J and R_s, operated as SEIG. In order to simulate their performance a stationary reference frame dq model including non-linear saturation and cross coupling effects is developed and verified experimentally. Several key investigations based on series capacitance selection, losses and efficiency, on-load performance with different power factor loads, transient performance with load perturbation and variable speed operation are carried out. The study reveals that SEIG with high J and lower R_s gives considerably better performance than its counterpart. The conclusions reported in the study are important especially for standalone/off grid application of SEIGs.

1. Introduction

A squirrel cage induction machine (SCIM) hosts electro-mechanical energy conversion in a self-excited induction generator (SEIG) system excited by optimum capacitance bank placed across its stator windings (Madvar et al., 2019). It is obvious that parameters of SCIM such as the stator winding resistance (R_s) and rotor inertia (J) are likely to have considerable impact on its performance as a SEIG. In-spite of this one finds almost no attempt to explore these specific aspects for a SEIG either in classical studies (Murthy et al., 1982; Chan, 1993) or the ones reported in recent past (Nasir and Daoud, 2020; Chauhan and Chatterjee, 2019). Present endeavor is undertaken to evaluate the affects of R_s and J of a SCIM on its performance as a SEIG.

Wind turbines are usually installed in remote and least accessible terrains which necessitates equipping them with rugged, fault tolerant, cost effective and maintenance free power generators (Shaqour et al., 2020). Such essential attributes made conventional synchronous generators out of favor for wind turbines as they entail stringent maintenance due to overheads like excitation system, brushes etc and are costly (Kumar and Vijayakumar, 2020).

Capacitor excitation of induction motors was identified in early 1900s (Bassett and Potter, 1935; Wagner, 1939). Subsequent developments paved way for introduction of SEIG (Mehmood et al., 2021). Squirrel cage structure of machine and capacitor excitation, doing away with brush and associated assembly, made the SEIG an immediate generator of choice for standalone power generating units like wind turbines supplying off grid loads (Khan and Khan, 2016).

Self-excitation of a SCIM depends on its magnetizing reactance, excitation capacitance and prime mover input speed (Ion, 2020). Initiation and sustenance of excitation in a SEIG are always detrimental to voltage build-up and its stabilization under different no-load and on-load operating conditions. Murthy (1993) and Murthy et al. (1993) laid out theory and experiments of a single-phase SEIG. Shridhar et al. (1995) make significant contribution on two accounts namely investigations on capacitor self-excitation and the load carrying capability for a SEIG including voltage regulation improvement by series capacitance (Khan et al., 2012).

Abbreviations: SCIM, squirrel cage induction machine; IG, induction generator; SEIG, self excited induction generator; PHIL, power hardware in loop; RL, resistive-inductive

* Correspondence to: Department of EE, Qatar University, Doha, Qatar.
E-mail address: atif.iqbal@qu.edu.qa (A. Iqbal).

https://doi.org/10.1016/j.egyr.2022.01.023

A fair account of progress made on various design, modeling, analyses and application aspects can be referred to the reviews of Induction generator (IG) systems carried out by Bansal (2005), Chauhan et al. (2010) and Singh (2004). Relatively recent developments in the induction machine designs have also been seamlessly extended to IGs. For instance, the multi-phase (more than three-phase) induction machines (Barrero and Duran, 2016) are successfully adopted in SEIG systems, six-phase IGs in particular have attracted attention off late (Khan and Khan, 2021). Recently in Liu et al. (2021) the power hardware in loop (PHIL) resources are employed for analysis of a SEIG equipped with the PHIL power electronic controllers to develop a SEIG emulator system.

Accurate assessment of the affects of SCIM parameters on its operation as SEIG can help in their performance optimization immensely. Some endeavors in this regard have been made in the available literature. Leicht and Makowski (2019) propose extension in operating range and quicker voltage build-up in a single-phase SEIG by rendering rectangular copper bars and round slots to its rotor. The performance improvement is apparently a result of increased skin effect and reduced deep bar effect in the rotor. Affects of rotor construction on the performance of a single-phase SEIG are simulated by Makowski and Leicht (2019). The study suggests applying rectangular copper rotor bars to be beneficial for obtaining greater steady state operating region for a SEIG.

Mathematical modeling is an integral part of realizing accurate behavior of physical systems. Levi and Rauski (1993) produced step by step procedure for developing mathematical model of a double- cage rotor SEIG. It is applicable to any law of shaft speed variation, regardless of the loading conditions, but the results presented are limited to self-excitation and no-load build-up.

Influence of magnetizing reactance, per-phase rotor resistance and reactance is accounted on the performance of a SEIG by Nigim et al. (2004). The study proposes employing optimally designed induction machines as IG rather than "off the shelf" ones. It is shown that driven by a regulated prime mover, an increase in rotor winding reactance of SEIG results in higher no-load generated voltage. On the other hand, an increase in rotor resistance causes decrease in generation frequency leaving the no-load voltage un-affected. No significant effect of varying the magnetizing reactance is observed. However, the conclusions of the analysis are based solely on simulation results and no experimental verification is carried out.

Inherently poor voltage regulation is a major operational constraint for SEIGs and is attributed to their inability to generate reactive power (Arthishri et al., 2017). The reactive power injected by optimum excitation capacitance bank alone is insufficient to support load voltage under different loading conditions along with exciting the SEIG windings (Khan and Khan, 2018). Thus, foremost operational requirement for a practically viable SEIG system is a suitable reactive power compensation scheme for load voltage regulation.

Research of past several decades has yielded number of strategies for voltage control of SEIGs (Kalla et al., 2020). Of these advanced power electronics based voltage controllers have attracted maximum interest in the recent past (Calgan and Demirtas, 2021; Calgan et al., 2020). Even though these controllers render accurate voltage control, switching of power electronic devices adversely affects the system reliability as frequent break downs may occur due to high frequency switching (Khan and Khan, 2021). In standalone and remote locations such a scenario could be catastrophic.

A simple, robust and reasonably successful method of load voltage regulation in SEIGs for standalone operation is by providing reactive power support through series capacitances in short shunt connection mode (Enany, 2017). It is well established that if chosen carefully and coordinated with speed and shunt capacitances, the series capacitances in a short shunt SEIG can maintain the load voltage almost constant over its entire working range from no-load to full load (Varshney et al., 2021). Besides, if the capacitors fail the replacement can be done on site from the plant spares without complete or prolonged shut down.

Present endeavor puts together outcome of a comprehensive study carried out to evaluate the affects of stator winding resistance (R_s) and rotor moment of inertia (J) on operating characteristics of a SEIG. Two distinctly designed SCIMs having substantially different R_s and J are deployed to get required performance indices. Influence of the parameters is assessed under steady state and transient operating conditions for no-load and on-load performance of SEIGs. The analysis is supported by simulation and experimental results combined with detailed comparative study of the SCIMs operated as SEIGs. Multiple machines are studied to gain a wider understanding on results as often mere simulations and validation on single machine lack generality. For the sake of adopting effective yet simple voltage regulation mechanism the series compensation, short shunt connection is employed. The simulation model of short shunt SEIG is developed considering the effects of magnetic saturation on SEIG parameters (Kiselychnyk et al., 2017).

The paper spans over nine sections: Section 1 outlines the contours of study, background and its relevance in view of state of the art. Section 2 delineates motivation and contributions of the study. Section 3 explains the methodology used. Section 4 presents mathematical modeling of SEIG considering saturation effect. Section 5 validates the developed simulation model with corresponding experimental results for *R* and *RL* loads. Section 6 studies parametric influence on steady state characteristics of SEIGs and their comparison. Section 7 assesses the affect of parameters on transient response of SEIGs. Section 8 proposes plan for future studies on the topic. Section 9 summarizes the main conclusions of study.

2. Motivation and contributions of the study

2.1. Motivation of proposed analysis

From the instances of research discussed in preceding section following shortcomings are observed in the realm of parametric influence analysis of a SEIG:

- The affects of SCIM parameters on its performance as SEIG are limited in scope and predominantly based on analytical studies.
- Steady state performance is presented in detail but transient analysis is restricted to voltage build-up and no-load analysis only.
- Conclusions drawn are specific to the machine considered for analysis and lack generalization.
- No case has so far been made to initiate a detailed study on the affects of rotor moment of inertia *J*, which may have considerable impact as the kinetic energy supplied by rotor is the source of input energy to SEIG.

2.2. Major contributions

- Effects of rotor inertia and stator winding resistance on the performance of SEIGs are accounted.
- Two SEIGs with different rotor inertia and stator winding resistance are studied through simulation and experimental results to draw generalized conclusions.

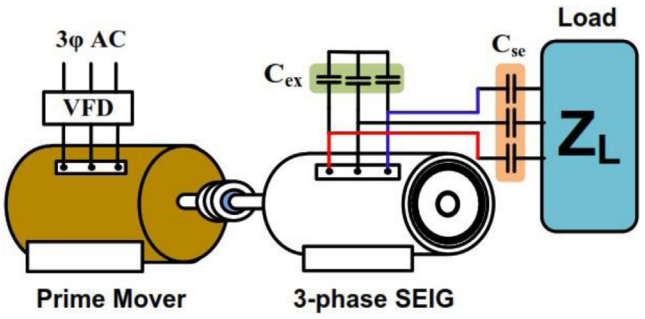

Fig. 1. 3φ-SEIG schematic with short shunt compensation connection.

Table 1
Parameter ratings of Induction Machines operated as SEIGs.

Parameters	Ratings for Machine-I	Ratings for Machine-II
V_{rated}, I_{rated}, P_{rated}	400 V, 5.5 A, 2.2 kW	415 V, 4.5 A, 1.5 kW
R_s, R_r	5.4 Ω, 1.7 Ω	12.6 Ω, 15.1 Ω
$X_{sl} = X_{rl}$, X_m	6.44 Ω, 251 Ω	20.3 Ω, 281 Ω
J, *Gross Weight*	0.0596 kg -m^2, 55 kg	0.012 kg -m^2, 22 kg

- Steady state and transient performance of SEIGs are extracted for different no load and on-load operating conditions with *R* as well as *RL* loads to carry out their parametric influence analysis.
- Effects of the studied parameters are analyzed on capacitance selection, losses and efficiency, variable speed operation and a host of other operating conditions and parameters for both the studied SEIGs.
- For analytical accuracy, the SEIG model is developed incorporating the affects of saturation on its parameters.

3. SEIG scheme and analysis methodology

Block schematic of the layout of short shunt SEIG employed in this study is illustrated in Fig. 1. The task of prime mover is entrusted with a 3φ induction motor fed by a variable frequency drive (VFD) which maintains the speed of prime mover and hence that of SEIG at 1500 rpm.

Excitation capacitance (C_{ex}) bank is connected in star configuration across the 3φ stator windings of SEIG. Star configuration of C_{ex} is chosen based as much on maintaining topographical consistency with star connected stator windings of SEIG as it is on convenience of available capacitors of appropriate values in laboratory. Alternatively, the capacitor bank can be connected in delta without any effect on SEIG performance. But in such a scenario the value of each capacitance shall be taken to be about $1/3_{\text{rd}}$ of each that is connected in star to keep per-phase capacitance same as in star configuration.

A series capacitance (C_{se}) is placed in each of the load terminals to inject capacitive vars in accordance with loading sustained by SEIG to regulate the load voltage.

In order to analyze the parametric influence of an induction machine on its operation as SEIG this study deploys a novel two machine analysis. For a practically viable outcome the study is conducted by analyzing experimental and simulation results obtained on two distinct induction machines designated as Machine-I and Machine-II both being operated as short shunt SEIG. Machine-I has low R_s and high *J* while Machine-II is selected with high R_s and low *J*. Both machines are of 3φ, star connected, 1425 rpm, 50 Hz, 4-pole specifications with the parameter ratings as mentioned in Table 1. Illustrations of experimental set-ups of both the Machines are depicted in Appendix.

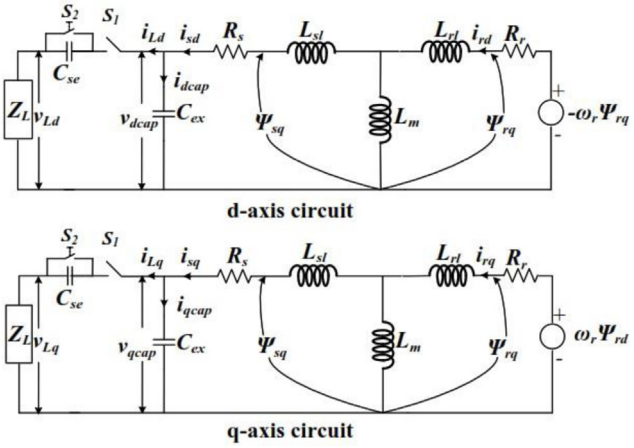

Fig. 2. DQ model of 3φ -SEIG.

4. Mathematical modeling of SEIG

Unlike motoring application, an induction machine relentlessly operates under magnetic saturation while rendering service as SEIG (Na et al., 2021). Saturation enforces steady state and stabilizes the voltage subsequent to a transient change in operating condition. This is typical behavior of a SEIG and is attributed to mismatch in its reactive power demand and supply from the capacitor bank. In this analysis the simulation model of studied 3φ-SEIG is developed including the non-linear saturation and cross coupling effects (Khan and Khan, 2021; Levi, 1994; Hallenius et al., 1991).

The dq model of a 3φ-SEIG with short shunt compensation connection incorporating various flux linkages is depicted in Fig. 2. By switching S_1 and S_2 ON and OFF various operating conditions of SEIG such as no-load, on load with and without series compensation are conveniently simulated.

Operating dynamics of the circuit shown in Fig. 2 may be expressed by a state–space equation given by (1)

$$\frac{d}{dt}\boldsymbol{i} = -\mathbf{L}^{-1}\mathbf{K}\boldsymbol{i} - \mathbf{L}^{-1}\boldsymbol{v} \tag{1}$$

Column vectors ***v, i*** and the matrices **L, K** are defined as:

$$\boldsymbol{v} = \begin{bmatrix} v_{dcap} & v_{qcap} & M^0_{rd} & M^0_{rq} \end{bmatrix}^T; \quad \boldsymbol{i} = \begin{bmatrix} i_{sd} & i_{sq} & i_{rd} & i_{rq} \end{bmatrix}^T;$$

$$\mathbf{L} = \begin{bmatrix} L_{slmd} & L_{dq} & L_{md} & L_{dq} \\ L_{dq} & L_{slmq} & L_{dq} & L_{mq} \\ L_{md} & L_{dq} & L_{rd} & L_{dq} \\ L_{dq} & L_{mq} & L_{dq} & L_{rq} \end{bmatrix};$$

$$\mathbf{K} = \begin{bmatrix} R_s & 0 & 0 & 0 \\ 0 & R_s & 0 & 0 \\ 0 & -\omega_r L_m & R_r & -\omega_r L_r \\ \omega_r L_m & R_r & 0 & \omega_r L_r \end{bmatrix};$$

4.1. Modeling of SEIG parameters

Different parameters of SEIG may be derived as follows:

4.1.1. Modeling of excitation and series capacitances

$$v_{dcap} = \frac{1}{C_{ex}} \int i_{dcap} dt + N^0_{dcap}$$
$$v_{qcap} = \frac{1}{C_{ex}} \int i_{qcap} dt + N^0_{qcap} \quad (2)$$

Series capacitance voltages may now be written as:

$$v_{dcse} = \frac{1}{C_{se}} \int i_{Ld} dt$$
$$v_{qcse} = \frac{1}{C_{se}} \int i_{Lq} dt \quad (3)$$

where, i_{qcap}=i_{sq}-i_{Lq} and i_{dcap}=i_{sd}-i_{Ld}.

4.1.2. Modeling of load

Load currents are evaluated as:

$$\frac{d}{dt} i_{Ld} = \frac{v_{dcap}}{L_L} - \frac{R_L}{L_L} i_{Ld} - \frac{R_L}{L_L C_{se}} \int i_{Ld} dt$$
$$\frac{d}{dt} i_{Lq} = \frac{v_{qcap}}{L_L} - \frac{R_L}{L_L} i_{Lq} - \frac{R_L}{L_L C_{se}} \int i_{Lq} dt \quad (4)$$

The load voltages are now expressed as:

$$v_{Ld} = v_{dcap} - v_{dcse}$$
$$v_{Lq} = v_{qcap} - v_{qcse} \quad (5)$$

As the operation of a SEIG is heavily dependent on its magnetic saturation characteristic it is imperative to incorporate the affects of non-linear saturation and cross coupling effects (Khan and Khan, 2021; Hallenius et al., 1991) in the developed model. In Levi (1994) it is meticulously explained that an approximation towards neglecting these effects may adversely reflect on the accuracy of the developed mathematical model of induction machine. Thus, non-linear saturation model of the SEIG is developed as follows (Levi, 1994; Hallenius et al., 1991):

$$L_m = \frac{|\Psi_m|}{|i_m|} \quad (6)$$
$$L = \frac{d|\Psi_m|}{d|i_m|} \quad (7)$$
$$L_{dq} = \frac{i_{md} i_{mq}}{|i_m|} \frac{dL_m}{d|i_m|} \quad (8)$$
$$L_{md} = L_m + (i_{md}/i_{mq}) L_{dq};\ L_{mq} = L_m + (i_{mq}/i_{md}) L_{dq} \quad (9)$$

Steady state saturated magnetizing inductance, L_m and dynamic inductance, L are expressed by (6) and (7) respectively.

It is worth mentioning here that the parameter L_{dq} represents cross coupling due orthogonal flux components and exists only due to saturation. Moreover, by setting L_{dq} =0 the saturation effect can be conveniently neglected from simulation model. Now, Eq. (6) may also be written as

$$|\Psi_m| = L_m |i_m| \quad (10)$$

Differentiating (10) both sides w. r. t $|i_m|$

$$\frac{d|\Psi_m|}{d|i_m|} = L_m + |i_m| \frac{dL_m}{d|i_m|} \quad (11)$$

Rearranging and substituting L=dΨ_m/d| i_m| from (7) yields following expression

$$\frac{dL_m}{d|i_m|} = \frac{L - L_m}{|i_m|} \quad (12)$$

L_{sl} and L_{rl} are stator and rotor leakage inductances.

$$L_{slmd} = L_{sl} + L_{md};\ L_{slmq} = L_{sl} + L_{mq} \quad (13)$$
$$L_{rlmd} = L_{rl} + L_{md};\ L_{rlmq} = L_{rl} + L_{mq} \quad (14)$$
$$L_r = L_{rl} + L_m \quad (15)$$
$$i_{md} = i_{sd} + i_{rd};\ i_{mq} = i_{sq} + i_{rq} \quad (16)$$
$$|i_m| = \left(i^2_{md} + i^2_{mq}\right)^{1/2} \quad (17)$$

Electromagnetic torque and mechanical equation of the SEIG are expressed respectively by (18) and (19)

$$T_e = \frac{3}{2}\frac{P}{2} L_m \left(i_{sq} i_{rd} - i_{sd} i_{rq}\right) \quad (18)$$
$$T_{mech} = J\frac{d\omega_r}{dt} + B_m \omega_r + T_e \quad (19)$$

5. Validation of developed SEIG model

The developed saturated model of SEIG is validated to establish its optimality for the proposed analysis. Experimental implementation of SEIG is achieved on a SCIM (designated as Machine-I) whose parameters are given in Table 1. In order to operate the SEIG in short shunt compensation mode as depicted in the working scheme of Fig. 1, the optimum excitation capacitance (C_{ex}) and series capacitance (C_{se}) values are selected as 15 μF and 40 μF respectively. The selected capacitance values are arrived at by performing tests on the SEIG and based on their ability to maintain load voltage stability for resistive as well as inductive loads.

For simulation modeling of SEIG the mathematical equations from (1) to (19) are implemented to get a robust simulation model for the short shunt SEIG incorporating the non-linear saturation and cross-coupling effects. It is worth mentioning here that magnetizing inductance (L_m) of the induction machine to be operated as SEIG is required to be evaluated for its analytical model. The L_m restores steady state after each transient change in operating condition of SEIG. For this study L_m is obtained by subjecting the induction machine to a standard test known as the "Synchronous Speed test" (Kalamen et al., 2012). Data obtained from the synchronous speed test is plotted and a polynomial given by (20) is obtained by fitting the plotted test data. From (20), L_m can be calculated for a given generated or load voltage of SEIG.

$$L_m = -9.1379\text{e}^{-14} V^5_{ph} - 1.2955\text{e}^{-10} V^4_{ph} - 6.1878\text{e}^{-8} V^3_{ph} - 8.4392\text{e}^{-6} V^2_{ph} - 8.2057\text{e}^{-5} V_{ph} + 1.065 \quad (20)$$

Both the resistive (R) and resistive–inductive (RL) loads are considered for the validation to gain better acceptability of the developed model. Simulation flowchart is depicted in Fig. 3.

5.1. SEIG supplying R load

Main area of application of the SEIGs is as a standalone power source for rural and far-off places deprived of electricity grids. Major utilization of electricity by the natives in these terrains takes place mainly for heating and lighting purposes which are predominantly resistive loads. Therefore, the R loads are important for performance analysis of any SEIG system. In order to assess the performance of studied SEIG it is loaded up-to its power rating of 2.2 kW. Experimental and simulated load voltage and current profiles are depicted in Fig. 4(a). It can be seen that the SEIG is able to supply the connected load at a load voltage and current of about 239 V(rms) and 3.2 A(rms) respectively. The load voltage THDs for experimental and simulated results are depicted in Fig. 4(b). The parameters are found to be converging quite satisfactorily within a tolerance of ±3%.

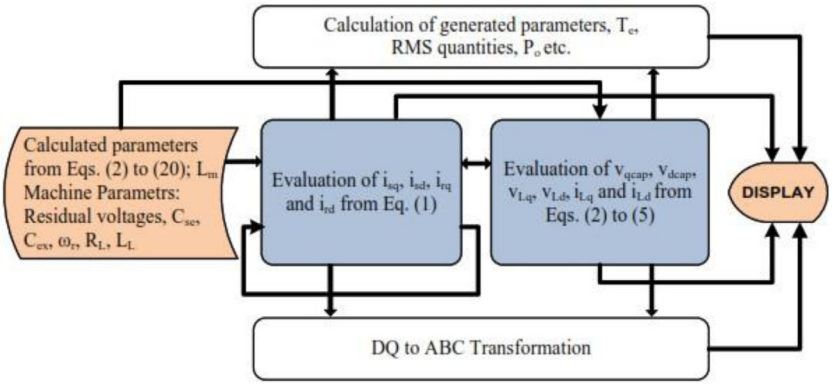

Fig. 3. Simulation flowchart for the short shunt SEIG analysis.

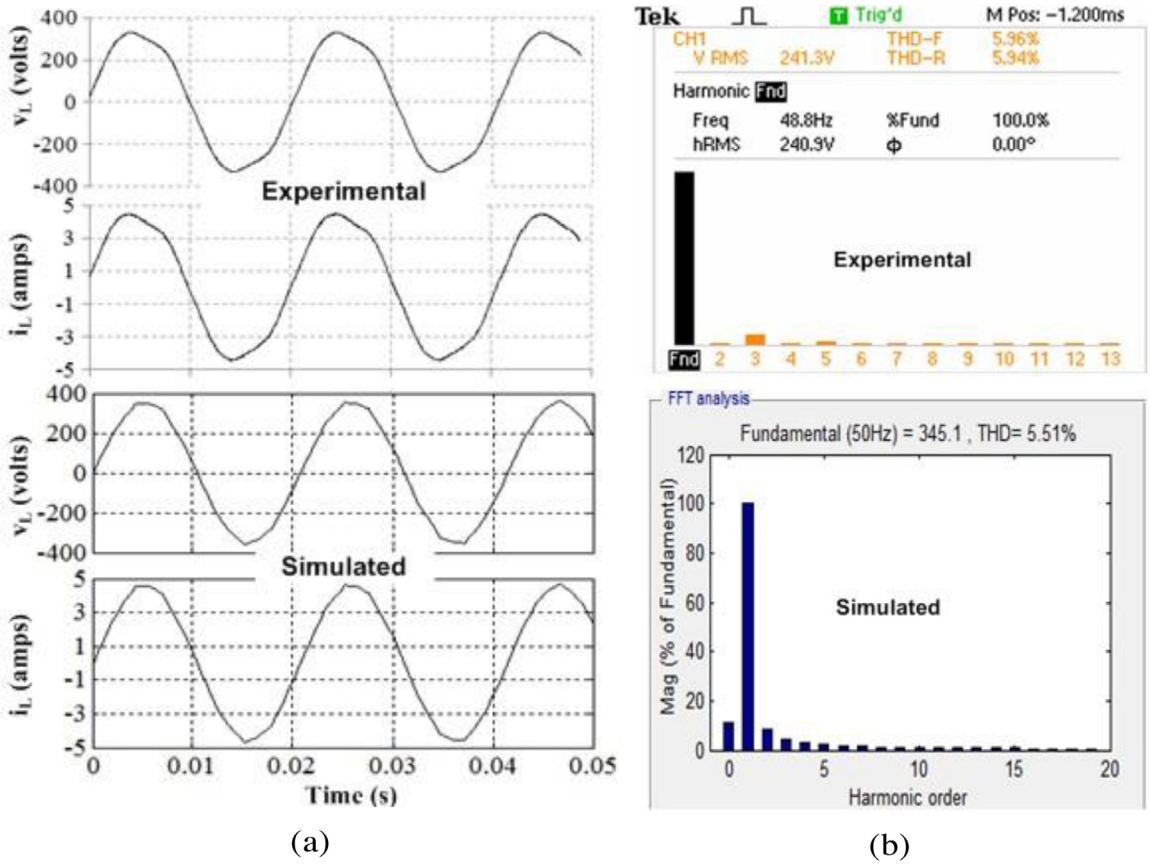

Fig. 4. Output parameters of Machine-I supplying unity PF load as short shunt SEIG (a) Experimental and simulated phase-A load voltage and current. (b) Experimental and simulated load voltage THD.

5.2. SEIG supplying RL load

Retaining the same set of optimum capacitances the rated load at 0.9 power factor (PF) lagging is now switched-on at the SEIG terminals with R_L=76 Ω and L_L=117 mH. As can be seen from Fig. 5(a) the full load simulated voltage is about 382.3 V(279 V, rms).

From the measured result the load voltage is obtained as 381.8 V (270 V, rms). The recorded and simulated currents are respectively 3.2 A and 3.13 A (rms). Reactive power drawn by the SEIG increases from 30.2 var/phase to 298 var/phase as the loading is changed from unity to 0.9 lagging i.e. an approximate 9 fold inflation is witnessed. The THDs of full load recorded and simulated voltages in the present case are illustrated by Fig. 5(b).

It is quite clear that the variation in load current is not much when compared with unity PF loading however a rise in load voltage at full load by more than 40 V is witnessed. This is quite common with capacitor excited and compensated SEIGs supplying *RL* loads (Khan et al., 2013; Khan and Khan, 2015). It so happens that as the R_L and L_L are decreased simultaneously to increase loading on the SEIG at same PF there comes a condition when the net inductive reactance becomes less than net capacitive reactance of the load branch of SEIG. This tends to create a condition wherein the SEIG operates overcompensated with regard to its reactive power resulting in rising load voltage.

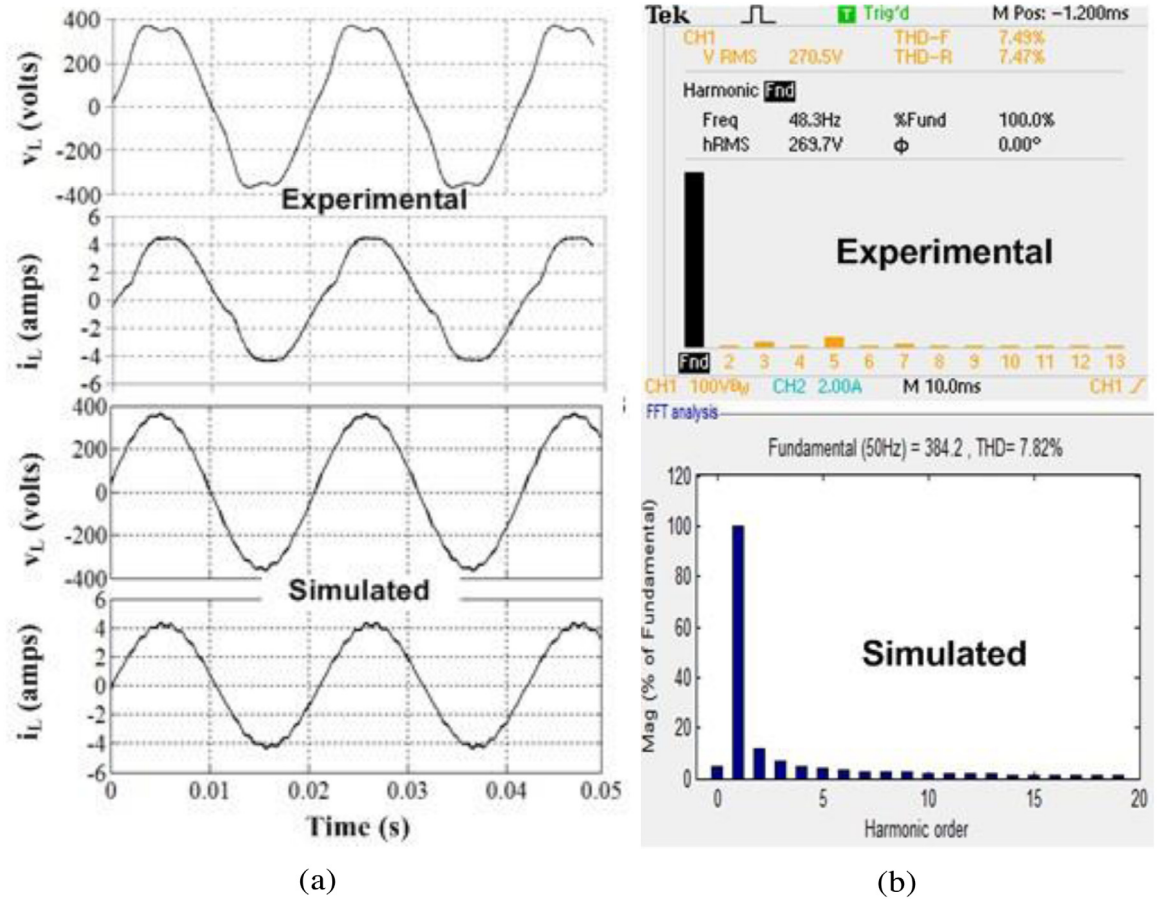

Fig. 5. Output parameters of Machine-I supplying 0.9 PF lagging load as short shunt SEIG (a) Experimental and (b) simulated phase-A load voltage and current. (b) Experimental and simulated load voltage THD.

5.3. Effect of incorporating saturation in the simulation model

To portray affects of saturation, the load voltage waveforms at 0.9 PF lagging with and without saturation effect are compared with experimental result in Fig. 6. Saturation effect can be easily suppressed from the developed simulation model by setting the parameter L_{dq}= 0 and L_{md} = L_{mq} = L_m. As can be seen from Fig. 6 the waveform of saturated model converges with experimental result more closely in terms of magnitude. The affect of saturation particularly manifests itself at the tips of voltage waveforms in the form of distortions as can be seen. Whereas saturated model replicates the same to a great extent the approximate model waveform is characterized by the absence of any such effect. However, it may be noted that there are minor discrepancies in simulating the distortions by saturated model since it is partially attributed to L load as well which is connected while recording the experimental results. Thus it is quite evident that saturated model results conform more closely to experimental ones.

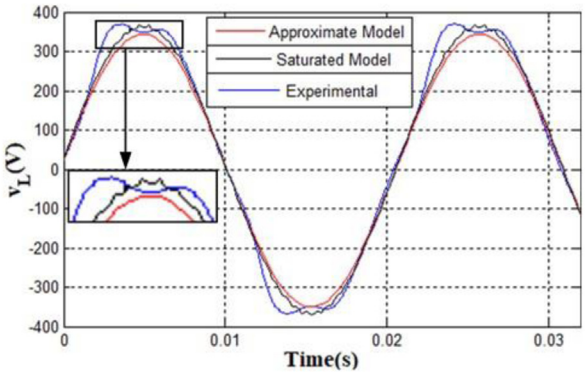

Fig. 6. Comparison of simulated load voltage waveforms of approximate and saturated model with experimental result of 0.9 lagging PF.

6. Proposed analysis

Response of both the machines is recorded for number of operating conditions in the ensuing sections to establish a comprehensive understanding on the affects of parameters considered for the analysis.

6.1. Variation of No-load Voltage (V_t) with stator winding resistance (R_s) of the Machines

Variations in no-load terminal voltage (V_t) of the Machines for different (R_s) are plotted in the simulated results of Fig. 7. It may be seen that although both the Machines show identically drooping response, the Machine-II voltage drops at a faster rate with increasing R_s than Machine-I. Owing to higher J the Machine-I is found to support its no-load voltage more as its voltage drops more gradually than Machine-II. The response of both the Machines can be obtained from (21) by substituting p_1 to p_4 for each Machine as shown in Fig. 7.

$$V_t = p_1 * R_s^3 + p_2 * R_s^2 + p_3 * R_s + p_4 \tag{21}$$

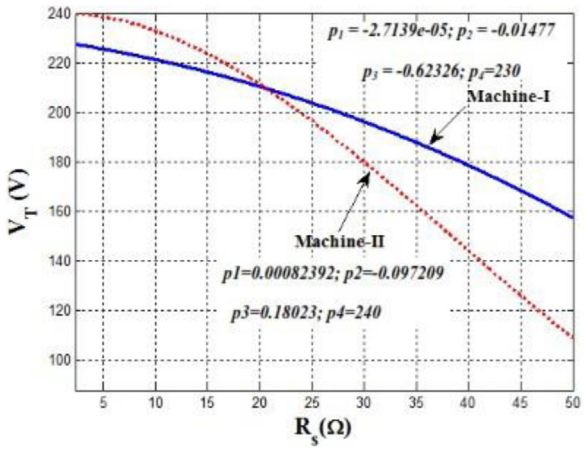

Fig. 7. Variation of V_t with R_s for the Machines.

6.2. Influence of parameters on the selection of series capacitance for the SEIGs

Series capacitance plays vital role of voltage compensation of SEIG under different load conditions. Therefore, it would be interesting to probe the influence of parameters under consideration for this study on the selection of series capacitance for SEIGs. Experimental variations in load voltage and output power with series capacitance for Machine-I and Machine-II supplying Unity PF load are shown in Fig. 8(a) and Fig. 8(b) respectively. The response of both the machines is identical in nature and follows the pattern of a quadratic function. An optimum series capacitance must yield best load voltage profile when supplying rated power.

The optimum series capacitance of Machine-I has already been evaluated as 40 μF earlier. For Machine-II as can be seen from Fig. 8(b) it comes out as 70 μF which is being combined the its optimum excitation capacitance which is 36 μF. It is observed that the optimum series capacitance for Machine-I exists just before the maxima of its characteristic in Fig. 8(a). However, for Machine-II it is found to be at maxima as depicted in Fig. 8(b). Thus, it is evident that the optimum series capacitance for a SEIG irrespective of its ratings, winding parameters and rotor inertia lies in the vicinity of maxima of its characteristics showing variation in V_L versus C_{se} or that of P_o with C_{se}.

Nonetheless, the two studied machines yield different optimum values for C_{se}. The machine with higher J and lower values of winding parameters i.e Machine-I has its optimum C_{se} =40 μF about half of 70 μF which is optimum for Machine-II. The lower value of C_{se} for Machine-I is due to its lower per-phase stator resistance (R_s) than Machine-II. With low R_s, Machine-I is found to suffer lower voltage drop as a fraction of its rated full load voltage. With low voltage drop, the Machine-I is certainly able to utilize the available reactive power more optimally than Machine-II. This results in lower C_{se} requirement for Machine-I compared to Machine-II. It is further observed from Fig. 8 that if output parameters of both the Machines are considered at any one optimum value say (40 μF) then both the Machines show contrasting results. As it is the optimum capacitance for Machine-I, it gives its best performance at this value in terms of load voltage regulation and output power. However, with same C_{se}=40 μF the Machine-II is able to generate only about 70% of its rated output power at a poor voltage regulation of about 16%.

6.3. Load voltage and stator current profiles

The external characteristics of Machine-I and Machine-II are respectively illustrated in Fig. 9(a) and Fig. 9(b). Both machines clearly exhibit the effect of series resonance due to series combination of *RL* load and on the full load voltages for Lagging load PFs. As a consequence, the load voltage of both machines is attaining progressively higher values for decreasing PF of the *RL* load near the rated loading. Therefore, regardless of machine parameters, rating, excitation/series capacitance values and other diversities, a short shunt SEIG will have higher load voltage for increasingly Lagging PF loads due to the inception of series resonance.

Further, the external characteristics of the two machines for unity PF case render contrasting results. This is of interest since SEIGs operating in isolated mode are most often expected to feed lighting and heating loads which are unity PF loads. This is why the optimum compensation (series) capacitance is selected with unity PF load. The full load voltage regulation of Machine-II is more than 18% which is off the mark from standard ±5% limit and the characteristic follows linearly drooping pattern. Against this, the full load voltage regulation of Machine-I is −3.9% which adheres to the ±5% limit while the characteristic is slightly meandering in nature having deviations between +4.3% and −6.9% from no-load to full load of 2200 W.

Machine-I, as can be seen, gives better output response than Machine-II for unity PF loading. A SEIG converts the kinetic energy of rotor to electrical energy with the reactive power being managed by capacitances. Now, since both the shunt and series capacitances are optimal, the performance of SEIGs is dependent on the input kinetic energy supplied by their rotors. Since both machines are driven at 1500 rpm the kinetic energy supplied by them in turn shall depend only on their respective values of J. From Table 1 it can be seen that the moment of inertia of Machine-I is almost 5 times that of Machine-II. Therefore, Machine-I has more energy input from the rotor side than Machine-II. The higher input enables Machine-I to give better response under loading condition as is evident from its results. The stator current of SEIGs increases with load and therefore defines threshold for safe loading limit. Any breach in the stator current limit results in overheating of the stator windings of SEIG.

The stator currents of Machine-I and Machine-II are plotted against output power in Fig. 10 for unity PF loading. It can be seen from the two characteristics of Fig. 10 that Machine-I utilizes stator current more judiciously than Machine-II. For instance, the rated no-load voltage of 230 V is established in Machine 1 at a stator current of 0.6 A, whereas Machine-II achieves 240 V on no-load with 2.9 A circulating in its stator windings. On the other hand, Machine-II supplies its rated power of 1500 W at almost its rated current of 4.5 A. But, working at similar current the Machine-I sets out its rated power of 2200 W which implies that it can be loaded further since its current rating is 5.5 A. Moreover, Machine-I generates about 500 W per Ampere of its stator current while Machine-II gives out 344 W for every Ampere rise in its stator current.

6.4. Losses and efficiencies of the machines

The preponderance of Machine-I has been observed from the above analysis and it also reflects in the copper losses of the machines. Copper losses of the two machines at half of full load (HFL) and full load (FL) are given in Table 2. The data in Table 2 reflects that if the losses are taken as the percentage of their rated powers, Machine-II incurs more losses than Machine-I. The copper losses of Machine-II are approximately 5 and 3 times higher than Machine-I at HFL and FL respectively taken as percentage of their respective rated powers. The per phase

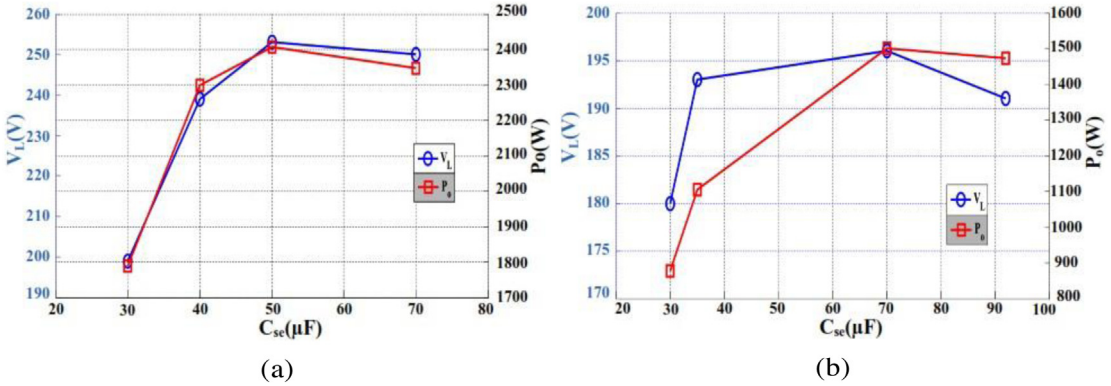

Fig. 8. Variation of load voltage and output power with series capacitance of (a) Machine-I and (b) Machine-II.

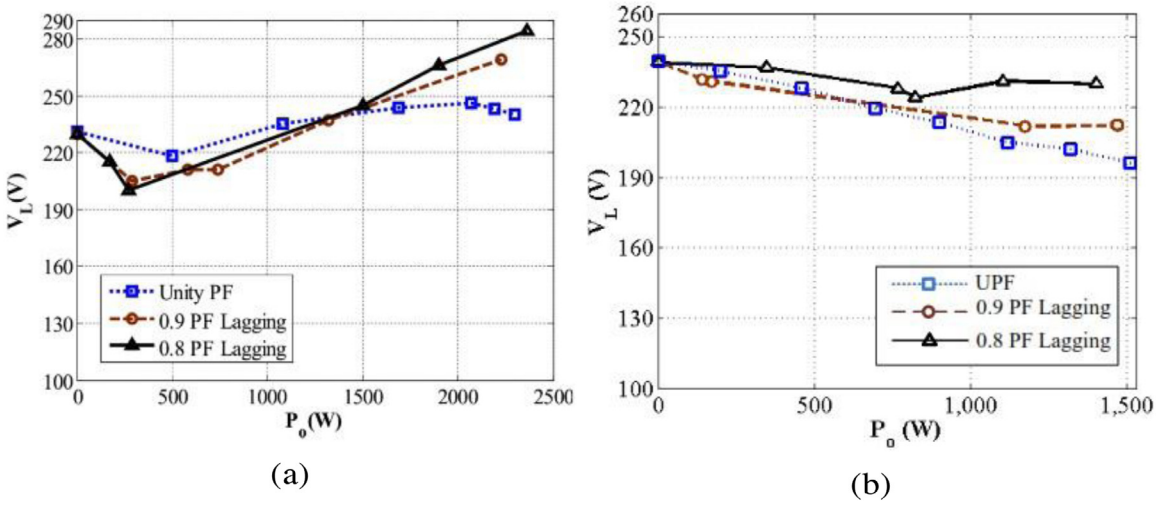

Fig. 9. External characteristics of (a) Machine-I and (b) For Machine-II.

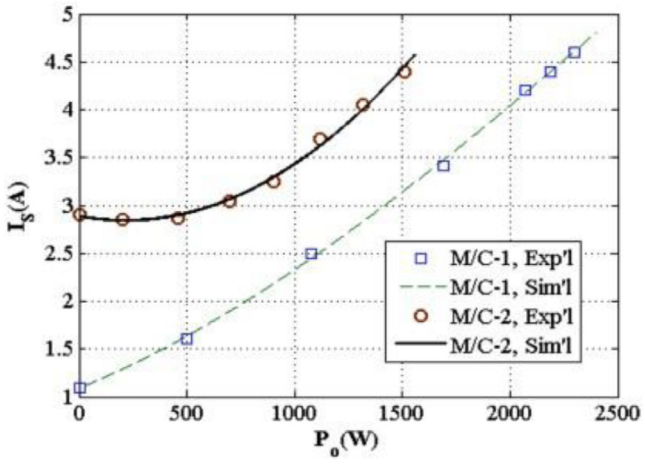

Fig. 10. Variation of stator current with output power of the two machines at unity PF.

Table 2
Copper losses of the Machines.

Connected Load	HFL		FL	
	Exp'l	Sim'l	Exp'l	Sim'l
Losses of Machine-I	101 W	99.6 W	342 W	344.2 W
Losses of Machine-II	337 W	341 W	702 W	718.8 W
As %age of power rating of each machine				
Losses of Machine-I	4.6%	4.5%	15.5%	15.6%
Losses of Machine-II	22.4%	22.73%	46.8%	46.9%

Table 3
Simulation events.

Event	Time
Application of load	t = 2 s
Speed reduced to 1125 rpm	t = 2.5 s
Speed increased to 1875 rpm	t = 5 s
Speed reduced to 1500 rpm	t = 8 s

winding parameters obviously play an important role in loss profile of the machines too. Lower R_s and better stator current profile are largely responsible for better copper loss profile of Machine-I than Machine-II. The efficiency versus load curves of the two machines are illustrated in Fig. 11 and clearly portray better performance of Machine-I as it supplies rated full load at about 19 percentage points higher efficiency than Machine-II.

7. Transient performance of the two machines

7.1. Effect of sudden load perturbation

The two machines are now assessed under load perturbation by sudden application of full load at unity PF to gain insights into

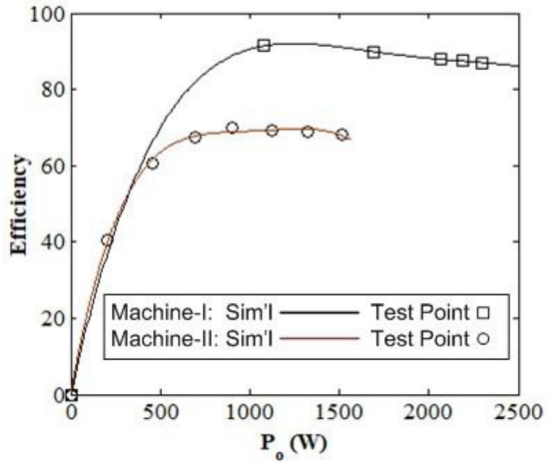

Fig. 11. Efficiency versus output power curves of the Machines.

their transient performance. Response of Machine-I and Machine-II in terms of their experimental load voltage waveforms can be seen in Fig. 12(a) and Fig. 12(b) respectively. Some interesting performance deviations are clearly visible from each load voltage profile. Firstly, as soon as load is switched-on for Machine-I at $t = 0.85$ s, the load voltage experiences a sudden transient dip. Subsequently, the voltage regains steady state at $t = 1.05$ s i.e in about 0.2 s with a good full load voltage regulation within 5% as already discussed. Contrary to this the response of Machine-II to sudden perturbation of full load is less in terms of momentary dip and more pronounced towards change in load voltage regulation. From Fig. 12(b) it is clearly seen that as the load is applied at $t = 0.64$ s the voltage dips but not to the extent it did in case of Machine-I. However, for Machine-II the full load voltage regulation is about 18% which is more than three times over the permissible limit of $\pm 5\%$.

7.2. Transient response of the machines under sudden change in input speed

Wind driven SEIGs are likely to encounter sudden changes in input speed especially when driven from wind turbines. To assess their response under transient changes in input speed both the machines are subjected to change in input speed while supplying rated power. Speed commands are issued in the simulation as per Table 3. Parameter variations for Machine-I and Machine-II are respectively illustrated in Fig. 13(a) and Fig. 13(b) for speed changes by $\pm 25\%$ of the rated value of 1500 rpm.

7.2.1. Speed decreased

The SEIG is loaded at $t = 2$ s by applying the rated unity power factor load and operates afterwards under loading for all changes in speed. It is observed that as the speed is reduced by 25% at $t = 2.5$ s from its rated value the load voltage ($\mathbf{v_L}$) and load current ($\mathbf{i_L}$) of Machine-I reduce respectively by 22% and 23% of their respective full load values. Likewise a reduction of 41% and 18% is seen respectively in output power ($\mathbf{P_o}$) and electromagnetic torque ($\mathbf{T_e}$). If the corresponding results of Machine-II are referred to, it is found that $\mathbf{v_L}$ and $\mathbf{i_L}$ drop by 55% and 56% of their full load values while $\mathbf{P_o}$ and $\mathbf{T_e}$ come down by 84% and 80%. It may also be seen that as soon as the speed is brought back to 1500 rpm both the machines are smoothly able to settle to their rated values.

Both the machines are found to regain steady state after each event of changing speed. However, there are some distinct traits exhibited by both which are replicated across all their output parameters. Firstly, it is observed that Machine-I responds to change in speed almost instantaneously and all the parameters adjust to the change quite rapidly. On the other hand the Machine-II parameters change more gradually subsequent to each variation of speed before settling down to new operating values. This is quite understandable and attributed to higher rotor inertia of Machine-I. As is already seen the value of J for Machine-I is about 5 times that of Machine-II as an implication the Machine-I decelerates much quickly compared to Machine-II. Also, it could be seen that in percentage terms the degree of reduction in the parameters of Machine-II is more than 2 times the corresponding parameters of Machine-I.

7.2.2. Speed increased

With input speed of both SEIGs still at 1125 rpm (25% less than 1500 rpm) a unit step command is given in the simulation to enhance the speed to 1875 rpm (25% higher than 1500 rpm) for both SEIGs. Referring to Fig. 13(a) and Fig. 13(b) one could clearly make out that the extent of variations in different parameters of both Machines are less prominent. If the variations are estimated from their base values at 1500 rpm it is found that $\mathbf{v_L}$, $\mathbf{i_L}$ and $\mathbf{P_o}$ of Machine-I increase respectively by 19%, 15% and 30% with negligible change in $\mathbf{T_e}$. On the other hand, the $\mathbf{v_L}$, $\mathbf{i_L}$, $\mathbf{P_o}$ and $\mathbf{T_e}$ of Machine-II increase respectively by 20%, 16%, 28% and 10%.

From the preceding discussion it is well established that both the Machines are quite sensitive to change in their input speed. But, for both Machines the parameters change to a greater extent when the speed is reduced as against the condition when speed is increased. This common nature is attributed to the fact that when fully loaded both Machines operate in the vicinity of their magnetic saturation while generating near rated voltage. Now, when the speed is reduced the degree of change in speed and hence the input power to SEIGs is reflected almost entirely on their generated parameters. Alternatively, when the speed is increased, even though input is increasing it does not reflect in its entirety on parameters as the Machines are already saturated and could not accommodate enhanced input in terms of increasing the output.

Notwithstanding their consonance in terms of overall behavior, there are specific deviations between the performance of two Machines. It is observed from the results that almost all the parameters of Machine-II display higher sensitivity to changes in speed either way compared to Machine-I. Both the Machines reflect quite similar changes when the speed is increased which may be attributed to the effect of saturation.

8. Scope for future investigations

Based on the concept of this study a number of investigations may be initiated to optimize wind powered generator designs. Some areas which require further exploring are mentioned below:

- Parametric influence analysis of SEIGs under grid connected operation.
- Development of new voltage and frequency control strategies for SEIGs.
- Utilization of multi-phase (more than three phase) machines attributes for performance optimization of SEIGs.
- Performance analysis and comparison of SEIGs driven by wind and hydro turbines.
- Replacement of excitation and series capacitances with an equally robust and simple non power electronics based technology for reactive power management of SEIGs.

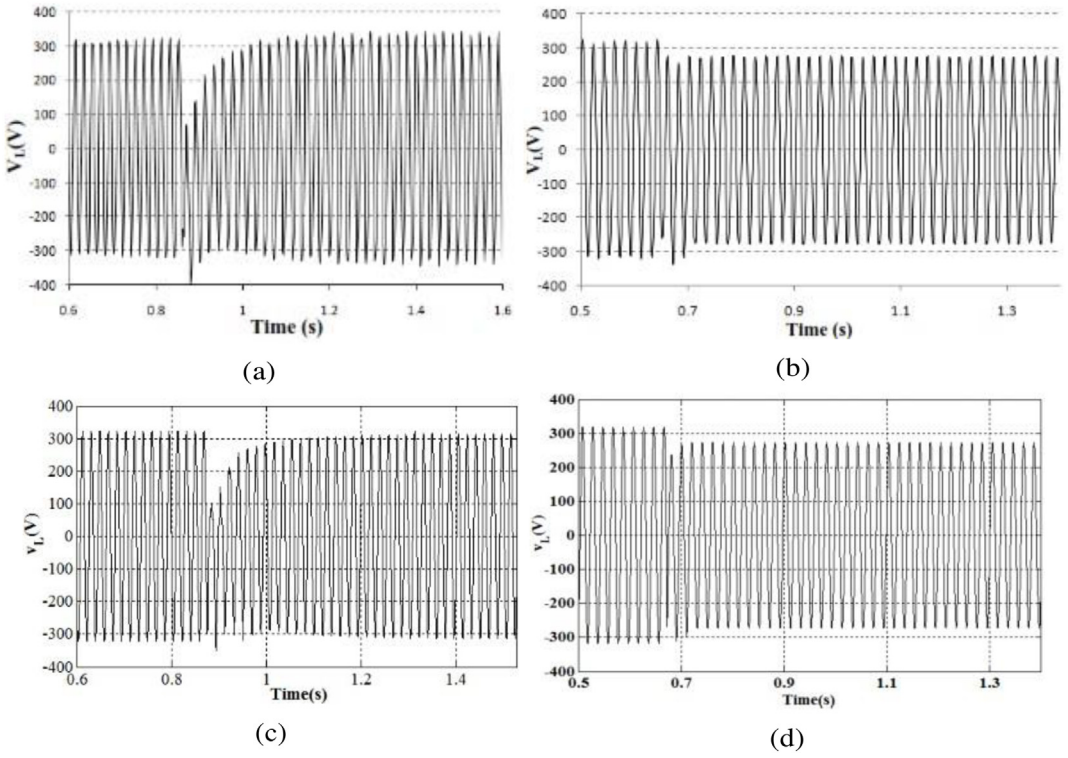

Fig. 12. Load voltage transients at rated unity PF loading for Machine-I; (a) Experimental, (c) Simulated and for Machine-II; (b) Experimental, (d) Simulated.

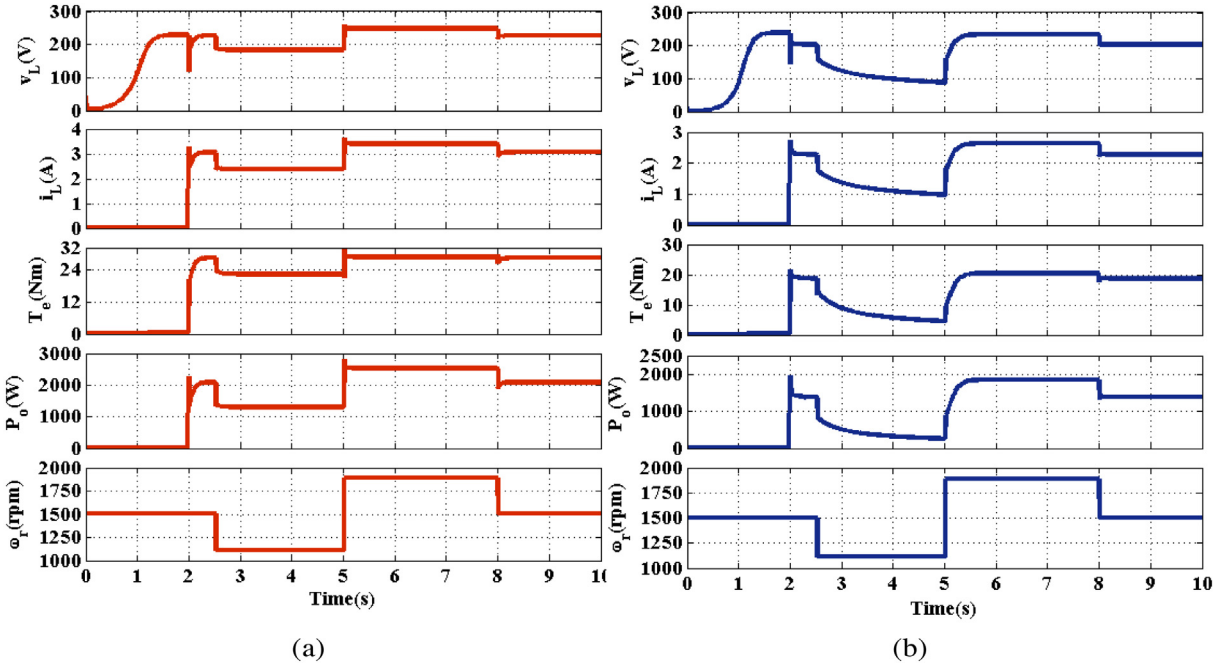

Fig. 13. Simulated parameters under input speed variations (a) for Machine-I and (b) for Machine-II.

9. Conclusion

Parameters of an induction machine (IM) affect its performance as a self excited induction generator (SEIG). In this study the effects of rotor moment of inertia (J) and winding resistance (R_s) values of an IM as SEIG are assessed. Simulation modeling, experimental validation and a novel comparison between two distinctly designed series compensated SEIGs with regard to their J and R_s is undertaken. Results reveal that Machine-I (having J about 5 times and R_s about half that of the other referred as Machine-II) exhibits better reactive power management as it keeps its load voltage almost constant with 40 μF series capacitance about half of 70 μF required by Machine-II. Machine-I is also found to augment about 40% higher active power per ampere rise in its stator current. These attributes lend better copper loss and efficiency profiles to Machine-I as it incurs about 1/3rd the copper loss and yields about 19 percentage points higher efficiency. Transient response of both the machines is

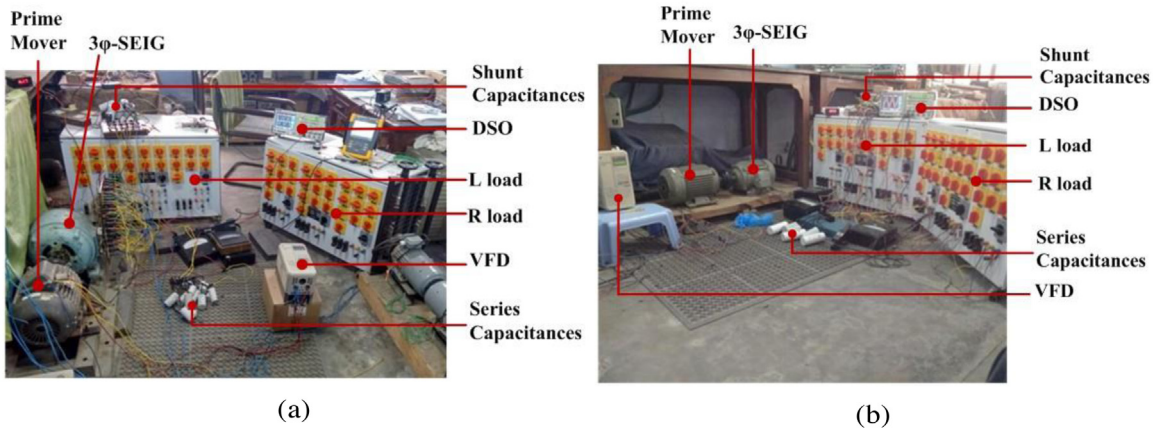

Fig. 14. Experimental setup of (a) Machine-I and (b) Machine-II.

assessed with load perturbation and variable speed operation where Machine-I is able to maintain its parameters more stable. Thus, it is found that SEIGs with higher J and lower R_s give more optimum performance.

Declaration of competing interest

The authors declare that they have no known competing financial interests or personal relationships that could have appeared to influence the work reported in this paper.

Acknowledgments

This publication was made possible by Qatar University Collaborative Research grant # [QUCG-CENG-21/22-1] from the Qatar University. The statements made herein are solely the responsibility of the authors. The APC for the article is funded by the Qatar National Library, Doha, Qatar.

Appendix

Nomenclature

Symbol	Description	Subscripts	Description
R	Resistance, Ω	l	Leakage quantities
C	Capacitance, μF	$d;q$	d; q axes quantities
L	Inductance, H	$L;NL$	Load; no-load mutual
N	Initial voltage, V	mu	Mutual capacitance parameters
M	Residual voltage, V	cap	Capacitance parameters
ψ	Flux, Wb	s/r	Stator/rotor quantities
ω	Speed, rad/s	ex/se	Excitation/series

Experimental setup of SEIGs

See Fig. 14.

References

Arthishri, K., Anusha, K., Kumaresan, N., Kumar, S.S., 2017. Simplified methods for the analysis of self-excited induction generators. IET Electr. Power Appl. 11 (9), 1636–1644.

Bansal, R., 2005. Three-phase self-excited induction generators: an overview. IEEE Trans. Energy Convers. 20 (2), 292–299.

Barrero, F., Duran, M.J., 2016. Recent advances in the design, modeling, and control of multi-phase machines part i. IEEE Trans. Ind. Electron. 63 (1), 449–458.

Bassett, E., Potter, F., 1935. Capacitive excitation for induction generators. Trans. Am. Inst. Electr. Eng. 54 (5), 540–545.

Calgan, H., Demirtas, M., 2021. A robust lqr-fopi λdμ controller design for output voltage regulation of stand-alone self-excited induction generator. Electr. Power Syst. Res. 196, 107175.

Calgan, H., Ilten, E., Demirtas, M., 2020. Thyristor controlled reactor-based voltage and frequency regulation of a three-phase self-excited induction generator feeding unbalanced load. Int. Trans. Electr. Energy Syst. 30 (6), e12387.

Chan, T.F., 1993. Capacitance requirements of self-excited induction generators. IEEE Trans. Energy Convers. 8 (2), 304–311.

Chauhan, P.J., Chatterjee, J.K., 2019. A novel speed adaptive stator current com pensator for voltage and frequency control of standalone seig feeding three-phase four wire system. IEEE Trans. Sustain. Energy 10 (1), 248–256.

Chauhan, Y.K., Jain, S.K., Singh, B., 2010. A prospective on voltage regulation of self-excited induction generators for industry applications. IEEE Trans. Ind. Appl. 46 (2), 720–730.

Enany, M.A., 2017. Series compensation assessment of self-excited induction generator using genetic algorithm. EPE J. 27 (1), 1–11.

Hallenius, K.-E., Vas, P., Brown, J., 1991. The analysis of a saturated self-excited asynchronous generator. IEEE Trans. Energy Convers. 6 (2), 336–345.

Ion, C.P., 2020. A comprehensive overview of singlephase self-excited induction generators. IEEE Access 8, 197420-197430.

Kalamen, L., Rafajdus, P., Sekerak, P., Hrabovcova, V., 2012. A novel method of magnetizing inductance investigation of self-excited induction generators. IEEE Trans. Magn. 48 (4), 1657–1660.

Kalla, U.K., Singh, B., Kumar, P., Agarwal, K.L., Murthy, S., 2020. State-of-the-art and comprehensive study of renewable energy sources based microgrid with single-phase self-excited induction generator. IET Renew. Power Gener. 18, 3699–3714.

Khan, M.F., Khan, M.R., 2015. Comprehensive analytical and experimental analysis of a self excited induction generator for renewable energy application. Int. J. Renew. Energy Res. (IJRER) 5 (3), 746–756.

Khan, M.F., Khan, M.R., 2016. Analysis of voltage build-up and speed disturbance ride through capability of a self-excited induction generator for renewable energy application. Int. J. Power Energy Convers. 7 (2), 157–177.

Khan, M.F., Khan, M.R., 2018. Generalized model for investigating the attributes of a six-phase self-excited induction generator over a three-phase variant. Int. Trans. Electr. Energy Syst. 28 (10), e2600.

Khan, M.F., Khan, M.R., 2021. Modeling and analysis of a six-phase self excited induction generator feeding induction motors. IEEE Trans. Energy Convers. 36 (2), 746–754.

Khan, M.F., Khan, M.R., Iqbal, A., 2012. Performance analysis of shunt, short shunt and long shunt self excited induction generator: Analysis of shunt, short shunt and long shunt seig. In: 2012 IEEE International Conference on Power Electronics, Drives and Energy Systems (PEDES). IEEE, pp. 1–6.

Khan, M.R., Khan, M.F., Iqbal, A., 2013. Investigation on resonating behaviour of a self excited induction generator. In: IEEE 2013 Tencon-Spring. IEEE, pp. 80–84.

Kiselychnyk, O., Bodson, M., Wang, J., 2017. Comparison of two magnetic saturation models of induction machines and experimental validation. IEEE Trans. Ind. Electron. 64 (1), 81–90.

Kumar, S., Vijayakumar, K., 2020. Simulation and experimental comparative analysis of the dc-dc converter topologies for wind driven seig fed dc nanogrid. Electr. Power Syst. Res. 181, 106196.

Leicht, A., Makowski, K., 2019. Influence of shape and material of rotor bars on performance characteristics of single-phase self-excited induction generators. COMPEL 38 (4), 1235–1244.
Levi, E., 1994. Applications of the current state space model in analyses of saturated induction machines. Electr. Power Syst. Res. 31 (3), 203–216.
Levi, E., Rauski, D., 1993. Modelling of deep-bar and double-cage self-excited induction generators for wind-electricity generation studies. Electr. Power Syst. Res. 27 (1), 73–81.
Liu, Y., Masadeh, M.A., Pillay, P., 2021. Power hardware-in-the-loop based emulation of a self- excited induction generator under unbalanced conditions. IEEE Trans. Ind. Appl. 1.
Madvar, M.D., Ahmadi, F., Shirmohammadi, R., Aslani, A., 2019. Forecasting of wind energy technology domains based on the technology life cycle approach. Energy Rep. 5, 1236–1248.
Makowski, K., Leicht, A., 2019. Comparative analysis of single-phase self-excited induction generators of various rotor cages. Electr. Eng. 101 (3), 805–812.
Mehmood, K., Cheema, K.M., Tahir, M.F., Saleem, A., Milyani, A.H., 2021. A comprehensive review on magnetically controllable reactor: Modelling, applications and future prospects. Energy Rep. 7, 2354–2378.
Murthy, S., 1993. A novel self-induced self-regulated single phase induction generator, i. basic system and theory. IEEE Trans. Energy Convers. 8 (3), 377–382.
Murthy, S., Malik, 0., Tandon, A., 1982. Analysis of self-excited induction generators. In: IEE Proceedings C (Generation, Transmission and Distribution). Vol. 129, IET, pp. 260–265.
Murthy, S., Rai, H., Tandon, A., 1993. A novel self-exited self-regulated single phase induction generator, ii. experimental investigation. IEEE Trans. Energy Convers. 8 (3), 383–388.
Na, W., Muljadi, E., Han, S., Tagayi, R.K., Kim, J., 2021. Possibility of power electronics-based control analysis of a self-excited induction generator (seig) for wind turbine and electrolyzer application. Electronics 10 (22), 2743.
Nasir, B.A., Daoud, R.W., 2020. Modeling of wind turbine-self excited induction generator system with pitch angle and excitation capacitance control. In: AIP Conference Proceedings. Vol. 2307, AIP Publishing LLC, 020022.
Nigim, K., Salama, M., Kazerani, M., 2004. Identifying machine parameters influencing the op- eration of the self-excited induction generator. Electr. Power Syst. Res. 69 (2–3), 123–128.
Shaqour, A., Farzaneh, H., Yoshida, Y., Hinokuma, T., 2020. Power control and simulation of a building integrated stand-alone hybrid pv-wind-battery system in Kasuga City, Japan. Energy Rep. 6, 1528–1544.
Shridhar, L., Singh, B., Jha, C., Singh, B., Murthy, S., 1995. Selection of capacitors for the self regulated short shunt self excited induction generator. IEEE Trans. Energy Convers. 10 (1), 10–17.
Singh, G.K., 2004. Self-excited induction generator research-a survey. Electr. Power Syst. Res. 69 (2–3), 107–114.
Varshney, L., Vardhan, A.S.S., Vardhan, A.S.S., Kumar, S., Saket, R., Sanjeevikumar, P., 2021. Performance characteristics and reliability assessment of self-excited induction generator for wind power generation. IET Renew. Power Gener..
Wagner, C., 1939. Self-excitation of induction motors. Electr. Eng. 58 (2), 47–51.